Tạp chí Khoa học và Công nghệ, Số 80, 2026

SINGLE PHASE GRID CONNECTED INVERTER CURRENT CONTROL METHOD BASED ON SMC WITH LCL FILTER

PHAM TRAN BICH THUAN [1*], NGUYEN VINH QUAN [2]

[1] Office of Science Management and International Affairs, Industrial University of Ho Chi Minh City, First Author;

[2] Faculty of Electronics Technology, Industrial University of Ho Chi Minh City, Member Author;

** Corresponding author: phamtranbichthuan@iuh.edu.vn*

DOIs: https://www.doi.org/10.46242/jstiuh.v80i2.5906

Abstract. A novel current control technique for a single-phase Neutral Point Clamped (NPC) multilevel inverter has been proposed, which is used to inject power into the grid and regulate the DC link voltage. The primary challenge lies in controlling the system due to the LCL filter's resonance and the difficulty in generating the filter capacitor's reference voltage. To address these issues, a novel Sliding Mode Control (SMC) algorithm is introduced, which inherently suppresses the LCL resonance without additional damping methods. The system employs a Multiple Loop Control (MLC) structure, featuring an outer current control loop and an inner proportional resonant (PR) voltage control loop. This inner loop effectively minimizes the capacitor voltage steady-state error and mitigates the SMC-induced chattering, thereby enhancing overall system performance and robustness. Furthermore, a hysteresis band switching technique with a dual frequency band is used for pulse generation. Simulation and experimental results, conducted on a three-level NPC T-type inverter, validate the effectiveness and robust performance of the proposed control strategy under varying conditions and external disturbances.

Keywords. Single Phase Inverter; Neutral Point Clamped inverter; Sliding Mode Control; Current Controller.

1 INTRODUCTION

Grid-connected inverters (GCIs) are essential components for integrating renewable energy sources into the electrical grid. Their primary functions include regulating the DC link voltage, controlling the power flow, ensuring low-harmonic power injection, and achieving perfect grid synchronization. In essence, inverters convert DC power (typically from storage) into AC power with the same frequency and phase as the grid voltage.

Numerous studies have explored control techniques for single-phase and three-phase GCIs, often utilizing methods like sinusoidal pulse width modulation (SPWM) [1, 2], specialized filter designs [3, 4], and phase-locked loops (PLLs) [5, 6]. Among the various control methods proposed to enhance power quality and exchange—such as current hysteresis control (CHC) [7, 8], voltage-oriented control (VOC) [9, 10], proportional-resonant (PR) control [11], and sliding mode control (SMC) [12, 13, 14]—CHC, VOC, PR, and SMC remain the most common. Methods to naturally minimize resonance in LCL filters have also been proposed in studies [15,16,17]. Although CHC is favored for its simplicity, fast dynamic response, and inherent robustness, its major drawback is the fluctuating switching frequency, which complicates filter design and implementation due to its dependency on system parameters and sampling frequency.

Sliding mode control (SMC) is widely recognized for its fast dynamic response and exceptional robustness to parameter uncertainties and noise, largely because it does not rely on a precise mathematical model of the inverter. This characteristic makes SMC highly attractive for applications where resilience is paramount. However, a major disadvantage of SMC is the chattering phenomenon caused by high-frequency switching. In contrast, the PR control method, while offering a fast decay response, is often criticized for its sensitivity and potential instability issues.

This paper proposes a novel current control technique for GCI based on Sliding Mode Control (SMC), incorporating an LCL filter. The proposed model-based control algorithm is designed for straightforward implementation in low-cost microcontroller systems. The algorithm inherently solves the LCL filter's resonance problem through SMC without requiring any additional damping techniques. Furthermore, the control strategy avoids the need for a complex PLL for synchronization and eliminates a separate modulation stage by directly employing a variable-switching-frequency hysteresis band technique. The use of a Multiple Loop Control (MLC) technique significantly reduces the SMC-induced chattering and minimizes the steady-state error, thereby improving overall system efficiency.

The remainder of this paper is organized as follows: Section 2 develops the mathematical model for the GCI with an LCL filter, formulates the sliding control law, and demonstrates the proposed algorithm's stability. Section 3 presents detailed simulation and experimental results, including the evaluation of the Normalized Root Mean Square Measure (NRMSE) for quantifying the fit between the setpoint and measured quantities. Finally, Section 4 concludes by highlighting the superiority of the proposed method, followed by the list of references.

2 THE MATHEMATICAL MODEL FOR THE GCI WITH AN LCL FILTER

2.1 Mathematical Model Gid-connected inverter with LCL filter

The circuit diagram of a single-phase grid-connected Voltage Source Inverter (VSI) with an LCL filter is shown in Figure 1. The primary function of the VSI is to deliver the required alternating current into the grid through appropriate switching of the four power switches from S1 to S4.

A single-phase three-level T-NPC inverter has a DC voltage source on the left and an uncertain grid on the right, connected through the LCL filter. Vin and $S_j (j = 1, 2, 3, 4)$ represent the DC voltage source and four switches, respectively. The complementary switching states are:

$$S1 + S3 = 1,\ S2 + S4 = 1 \tag{1}$$

There are a total of four operating modes. If n is the number of levels, the output voltage Vin of the inverter has three levels: +Vin, -Vin, and 0.

On the other hand, the main function of te LCL filter is to reduce high-frequency ripple caused by the current switching of the grid as shown in Figure 1. The LCL filter consists of an inverter-side inductor L1, a grid-side inductor L2, and a capacitor C connected in parallel. The differential equations of the system can be written as follows:

$$L_1 \frac{di_1}{dt} = uV_{in} - v_c \tag{2}$$

$$L_2 \frac{di_2}{dt} = v_c - v_g \tag{3}$$

$$C \frac{dv_c}{dt} = i_1 - i_2 \tag{4}$$

Where $v_g = V_g \sin(\omega t)$ is the grid voltage, i_1 is the inverter current, i_2 is the grid current, v_C is the capacitor voltage, V_{in} is the DC input voltage, and is the input control signal, with values in the finite set $\{-1, 0, 1\}$. The error variables can be defined as:

$$x_1 = v_c - v_c^* \tag{5}$$

$$x_2 = \frac{dv_c}{dt} - \frac{dv_c^*}{dt} \tag{6}$$

$$x_3 = i_2 - i_2^* \tag{7}$$

Where v_C^* and i_2^* are set values of v_c and i_2, respectively.

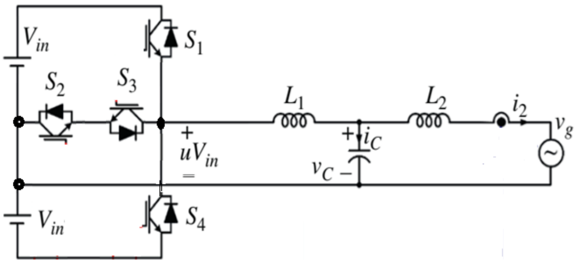

Figure 1: VSI single phase connected with LCL filter.

In grid-connected inverter systems, both active and reactive power control are necessary. In the case of active power control, the current injected into the grid must be sinusoidal and predominantly in phase with the grid voltage. To meet this requirement, the reference signal i_2^* must be determined as:

$$i_2^* = I_2^* \sin(\omega t) \tag{8}$$

By using equation (8), v_C^* can be generated in the following form:

$$v_c^* = L_2 \frac{di_2^*}{dt} + v_g \tag{9}$$

2.2 Design the Sliding Control Law

The proposed sliding surface equation:

$$s(x) = c_1 x_1 + c_2 x_2 + c_3 x_3 \tag{10}$$

with $c_1, c_2, c_3 > 0$ to ensure the stability of the close-loop systems, the error variables x_1, x_2 and x_3 are given by equations (5), (6) and (7). Substituting the equations for i_2 and i_2^* obtained from equations (3) and (9) into equation (7), we obtain x_3:

$$x_3 = \frac{1}{L_2} \int x_1 dt \tag{11}$$

Note that the integral in (11) eliminates the steady-state error in i_2 and v_C. In sliding control, using the Lyapunov stability theorem, the sliding surface must be zero ($s(x) = 0$). In this case, the error variables move on the sliding surface toward the equilibrium points (at the origin) ($x_1 = 0, x_2 = 0$ and $x_3 = 0$), the main goal here is for the inverter to achieve global asymptotic stability around these equilibrium points. However, the state trajectory will reach the sliding surface, satisfying the condition for asymptotic stability: the derivative of the Lyapunov function must be negative [18, 19, 20].

$$\frac{dV(x)}{dt} = s(x) \frac{ds(x)}{dt} < 0 \tag{12}$$

The time derivative of the sliding surface gives us:

$$\frac{ds(x)}{dt} = c_1 \frac{dx_1}{dt} + c_2 \frac{dx_2}{dt} + c_3 \frac{dx_3}{dt} \tag{13}$$

Taking the time derivatives of the error variables x_1, x_2 and x_3:

$$\frac{dx_1}{dt} = x_2 \tag{14}$$

$$\frac{dx_2}{dt} = \omega_1^2 u V_{in} - \omega_2^2 x_1 + D(t) \tag{15}$$

$$\frac{dx_3}{dt} = \frac{x_1}{L_2} \tag{16}$$

With $\omega_1 = 1/L_1 C$ and $\omega_2 = 1/L_2 C$, disturbance distribution $D(t)$ and ω_r as the resonant angular frequency of the LCL filter:

$$\omega_r = \sqrt{\frac{L_1 + L_2}{L_1 L_2 C}} \tag{17}$$

Since the sliding surface $s(x) = 0$ in the sliding mode, using equations (13), (14) and (16), we can obtain:

$$\frac{d^2 x_1}{dt^2} + \propto \frac{dx_1}{dt} + \frac{\beta}{L_2} x_1 = 0 \tag{18}$$

With $\propto = c_1/c_2$, $\beta = c_3/c_2$

The second-order differential equation (18) has solution:

$$x_1(t) = A_1 e^{p_1 t} + A_2 e^{p_2 t} \tag{19}$$

Where A_1 and A_2 are arbitrary constants, p_1 and p_2 are the poles of the closed-loop system given by the equation (20):

$$p_{1,2} = \frac{-\propto L_2 \pm \sqrt{\propto^2 L_2^2 - 4 L_2 \beta}}{2 L_2} \tag{20}$$

Clearly, the poles are real and located in the left half of the complex plane when $\propto^2 L_2^2 > 4 L_2 \beta$. In this case, $x_1(t) \to 0$. Hence, according (14) – (16), $x_2(t) \to 0$ and $x_3(t) \to 0$, the system is stable. Now, if we choose the control input u(t) to be the sign function:

$$u(t) = -\mathrm{sign}(s(x)) \tag{21}$$

Then, the condition (12) holds for the following cases: $+s(x) < 0 \Rightarrow u = 1$.

$$l_1 = \frac{ds(x)}{dt} = -\left(\omega_r^2 - \frac{\beta}{L_2}\right) x_1 + \alpha x_2 + d_1(t) > 0 \tag{22}$$

$+s(x) < 0 \Rightarrow u = -1$.

$$l_2 = \frac{ds(x)}{dt} = -\left(\omega_r^2 - \frac{\beta}{L_2}\right) x_1 + \alpha x_2 + d_2(t) > 0 \tag{23}$$

With:

$$d_1(t) = \omega_1^2 V_{in} + D(t) \tag{24}$$

$$d_2(t) = -\omega_1^2 V_{in} + D(t) \tag{25}$$

Equations (22) and (23) represent two parallel lines that form the boundaries of the stability region of the asymptotic mode. This region defined by l_1 and l_2, is illustrated in Figure 2. It is clear that the entire area consists of two distinct small regions. One region is located above the sliding surface ($s(x) = 0$), while the second region is below the sliding surface $s(x) = 0$. This sliding mode exists when the state trajectory intersects the sliding surface common to both regions. From Figure 2, it is easy to observe the line segment connecting the two points p_1 and p_2.

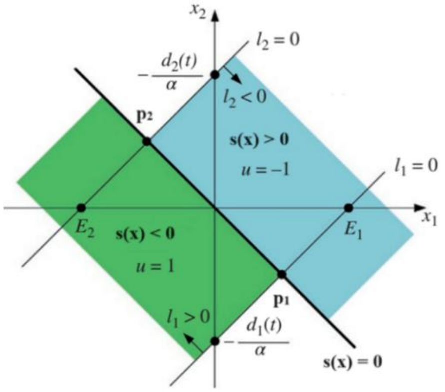

Figure 2: Stability regions of the asymptoic mode for $\beta < L_2\omega_r^2$

The intersection points with the x_1 axis of the lines l_1 and l_2 can be written as:

$$E_1(t) = \frac{L_2 d_1(t)}{L_2\omega_r^2 - \beta} \quad , \quad E_2(t) = \frac{L_2 d_2(t)}{L_2\omega_r^2 - \beta} \tag{26}$$

The lines l_1 and l_2 are parallel, which implies that their slopes are equal as follows:

$$m_1 = m_2 = \frac{1}{\propto}\left(\omega_r^2 - \frac{\beta}{L_2}\right) \tag{27}$$

The slopes m_1 and m_2 become postitive when $\beta < L_1\omega_r^2$, However, it should be noted that m_1 and m_2 no longer positive when $\beta > L_1\omega_r^2$ and $\beta = L_1\omega_r^2$, altering the boundary of the stability. When the boundary of the stability region is changed, the stability of the entire system is affected.

Through anslysis, we find that the stability of the entire system heavily depends on the parameters L_1, L_2 and C, which are nonlinear and time varying. Moreover, the sign(.) function can cause chattering, which degrades the quality of the inverter output. Therefore, in this paper, the authors recommened choosing the control law as the sliding mode $u(t) = s(x)$. This show that, from the equation (10), the stability of the entire system depends only on the pre-selected constants c_1, c_2 and c_3, allowing for the selection of desired pole pairs to reduce harmonics in the voltage and current before feeding it into the grid and to enhance the robustness of the controller, which will be disscussed in the follwing sections.

2.3 Design HW hysteresis switching

The triggering pulses for switches $s_1 \rightarrow s_4$ are generated from the HW hysteresis switching comparision between the sliding surface $s(x)$ and the threshold h.

To achieve a three-level output voltage for the inverter, a dual-band hysteresis modulation schme as show in (28, 29) is used.

$$S_1 = \begin{cases} 1, & \text{if } s(x) < -h \\ 0, & \text{Otherwise} \end{cases} \tag{28}$$

$$S_2 = \begin{cases} 1, & \text{if } s(x) < h \\ 0, & \text{Otherwise} \end{cases} \tag{29}$$

HW - Hysteresis Switching is illustrated in Figure 3. Clearly, the sliding surface $s(x)$ varies between the upper and lower boundaries of the hysteresis threshold h.

Table 1 shows the switching logic where h is the width of the hysteresis band. When the sliding surface $s(x) > 0$ in one half-cycle, switching is performed between S_1 and S_3 of the inverter. Similarly, when the sliding surface $s(x) < 0$ in the other half-cycle, switching occur for S_2 and S_4 of the inverter. An important consequence of using the dual-band hysteresis scheme is that all switching devices have equal switching losses in one cycle. On the other hand, while S_3 and S_4 have equal conduction losses in one cycle, S_1 and S_2 have no conduction losses except during the half-cycle when they are ON and OFF.

Table 1: Switching Logic

Output	Condition	$[S_1, S_2, S_3, S_4]$
$+V_{dc}/2$	$s(x) < -h$	[1,1,0,0]
$-V_{dc}/2$	$s(x) < +h$	[0,1,1,0]
0	$s(x) > 0, s(x) < 0$	[0,0,1,1]

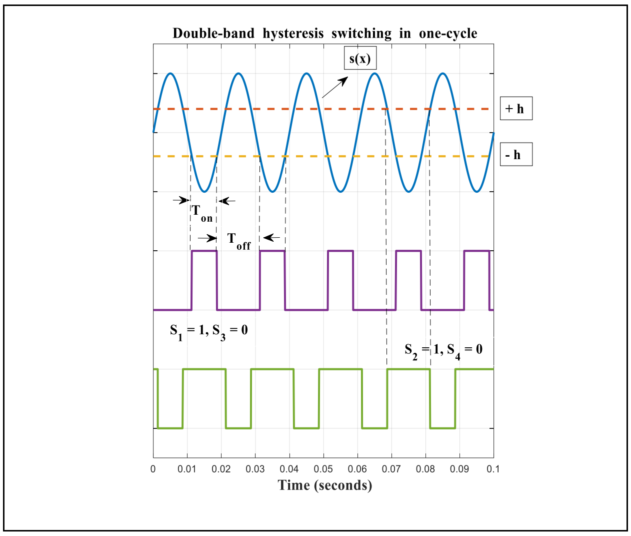

Figure 3: Dual-band hysteresis switching in one cycle

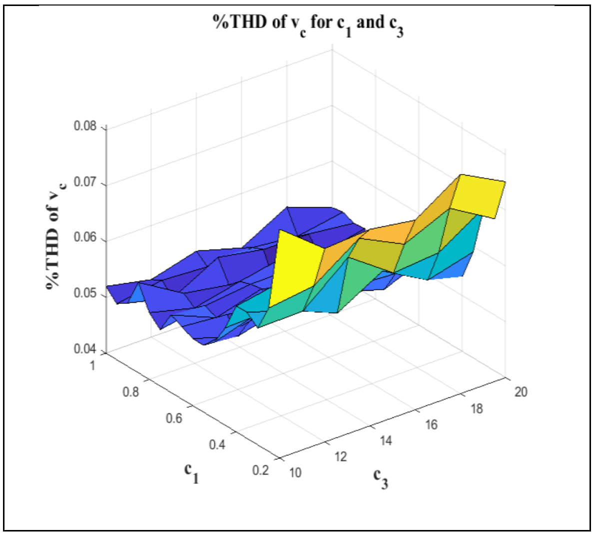

Figure 4: %THD of v_c for c_1 and c_3

Figure 4 is a graph representing the function $v_C = f(c_1, c_3)$, showing the impact of control gains c_1, c_2 and c_3 on the output quality of the inverter.

The minimum of the function, which corresponds to a harmonic THD = 0.047% of the capacitor voltage v_C, is achieved with $c_1 = 0.45$ and $c_3 = 20$. From equation (20), if choose $L_2 = 5mH$ and $c_2 = 0.5.10^{-4}$, we obtain the dominant poles of the close-loop system before compensation as $p_{1,2} = -2250 \pm j5900$.

2.4 Calculation of switching frequency

The relationship between switching frequency, hysteresis, and other parameter is very important and needs to be studied for practical applications. Here, the calculation of switching frequency is based on the assumption that state variables x_1 and x_2 are negligible in steady-state conditions. Substituting equations (14), (15) and (16) into (13) and assuming that $x_1 \approx 0$ and $x_2 \approx 0$, we can obtain the following approximate equation [14]:

$$\frac{ds(x)}{dt} \approx \omega_1^2 uV_{in} - K_d \sin(\omega t + \emptyset) \tag{30}$$

with $u = s(x)$, and:

$$K_d = \sqrt{v_g^2(\omega_1^2 - \omega^2)^2 + (\omega L_2 I_2^*)^2(\omega_r^2 - \omega^2)^2} \tag{31}$$

$$\emptyset = \tan^{-1}\left(\frac{\omega L_2 I_2^*(\omega_r^2 - \omega^2)}{v_g(\omega_1^2 - \omega^2)}\right) \tag{32}$$

The expressions for T_{on} and T_{off} can be written using Figure 3 as follows:

$$T_{on} = \frac{h}{\left.\frac{ds(x)}{dt}\right|_{s=1}} = \frac{h}{\omega_1^2 V_{in} - K_d \sin(\omega t + \emptyset)}$$

(33)

$$\mathrm{T_{off}} = \frac{-\mathrm{h}}{\left.\frac{\mathrm{ds(x)}}{\mathrm{dt}}\right|_{\mathrm{s}=0}} = \frac{\mathrm{h}}{\mathrm{K_d}\sin(\omega \mathrm{t}+\emptyset)} \tag{34}$$

Similarly, the phase deviation ϕ is negligible because: $\omega \mathrm{L_2 I_2^*}(\omega_r^2 - \omega^2) = \mathrm{v_g}(\omega_1^2 - \omega^2)$.

It should be noted that the sum of $\mathrm{T_{on}}$ and $\mathrm{T_{off}}$ creates the switching time for $\mathrm{S_1}$ and $\mathrm{S_2}$ in a half-cycle, while $\mathrm{S_3}$ is off and $\mathrm{S_4}$ continuously on. The switching period of the inverter in one cycle is twice $\mathrm{T_{sw}} = \mathrm{T_{on}} + \mathrm{T_{off}}$. Therefore, the instantaneous switching frequency equation within one cycle can be written as:

$$\mathrm{f_{sw}} = \frac{1}{2(\mathrm{T_{on}}+\mathrm{T_{off}})} = \frac{\mathrm{K_d}}{2\mathrm{h}\omega_1^2 \mathrm{V_{in}}}\left[\omega_1^2 \mathrm{V_{in}} \sin(\omega \mathrm{t}) - \mathrm{K_d}\sin^2(\omega \mathrm{t})\right] \tag{35}$$

The average switching frequency expression within one cycle can be written as:

$$\mathrm{f_{sw}} = \frac{\mathrm{K_d}}{\mathrm{h}\pi} - \frac{\mathrm{K_d^2}}{4\mathrm{h}\omega_1^2 \mathrm{V_{in}}} \tag{36}$$

The threshold of h and the value of $\mathrm{L_1}$ significantly affect the average switching frequency.

2.5 Control gain selection

When the system is in sliding mode, the non-idea state variable is not zero, and the sliding surface must satisfy $s(x) = 0$. Equation (20) provides approximate values for the closed-loop poles.

Nevertheless, the value of $\mathrm{c_1}$ and $\mathrm{c_3}$ can be chosen to place the poles at the desired locations, with the requirement that the total harmonic distortion of the capacitor voltage $\mathrm{v_C}$ and the grid current $\mathrm{i_2}$ is less than 0.1%. Choosing $\mathrm{c_1} = 0.3$, $\mathrm{c_2} = 0.5.10^{-4}$ and $\mathrm{c_3} = 20$ from equation (20). If $\mathrm{L_2} = 5\mathrm{mH}$ is chosen, the dominant poles of the closed-loop system after adjustment are $\mathrm{p_{1,2}} = -3000 \pm \mathrm{j}8426$.

Figure 5 shows the pole plot before adjustment (in blue) and after adjustment (in red). Two pairs of complex conjugate poles have negative real parts, so they lie on the left side of the imaginary axis, indicating that the system is table. Note that the smaller β, the closer the poles move to the imaginary axis, and the smaller α, the closer the poles move to the real axis, leading to increased system instability. Therefore, the pair of determining poles after adjustment will make the system stable.

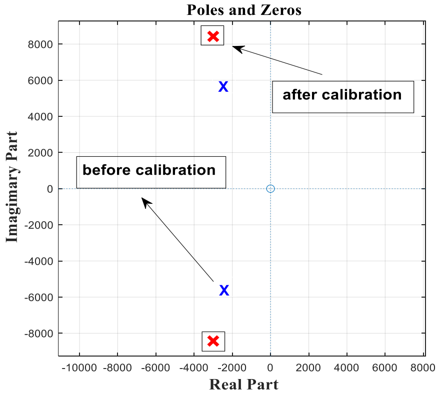

Figure 5: Poles and zeros plot

3 SIMULATION AND EXPERIMENTATION

The block diagram for the single-phase grid-connected VSI based on SMC is shown in Figure 6. The system calculates the sliding surface using Equation (10) and generates the switching signals via the dual-band hysteresis switching logic summarized in Table 1.

The results evaluate the compatibility between the reference $\mathrm{y^*}$ and the measured signal y, given by (37), with $\mathrm{mean(y)}$ being the average value of y:

$$\mathrm{NRMSE} = 100\left(1 - \frac{\|\mathrm{y^*}-\mathrm{y}\|}{\|\mathrm{y^*}-\mathrm{mean}(\mathrm{y^8})\|}\right) \tag{37}$$

The objective here is to implement a robust controller that can achieve high performance around the operating point (e.g., overshoot, settling time, and limited output harmonics) when there is a change in the input reference current, and invariant dynamic performance under different operating conditions.

The system's performance is tested under various conditions such as changes in the reference current i_2^* and unforeseen variations of unknown components, including the random distribution $D(t)$ inherently present in the system. The system parameters used in the simulation and experiment are given in Table 2.

The results present the response of the output voltage and the current through the inductor L_2 when the quantities i_2^* change. THD analysis and the NRMSE compatibility index for the voltage v_c and the grid current i_2 with their set values i_2^* and v_g. The solid lines in the graph represent the reference values of the gird current i_2^*, the gird voltage v_g and the dash lines represent the measured values of the gird current i_2 and the voltage across the capacitor v_c.

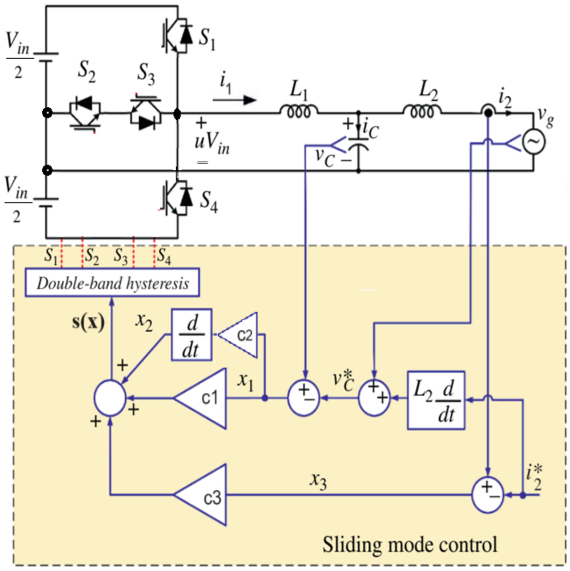

Figure 6: The block diagram of single-phase grid-connected VSI with the SMC method

Table 2: Simulation and Experiment parameters

Symbol	Value
DC link voltage, V_{in}	800 V
Set value, i_2^*	10 V
Grid voltage amplitude, v_g	$230\sqrt{2}$
Grid frequency, f_g	50 Hz
Inductance, L_1, L_2	5 mH
Filter capacitance, C	50 µF
Control Gains, c_1	0.3
Control Gains, c_2	$0.5.10^{-4}$
Control Gains, c_3	20
Band hysteresis, h	0.4
Time sampling, T_s	10 µF

3.1 Simulation results

Figure 7 represents the phase voltage at the output of the inverter when using the dual-band hysteresis modulation scheme, showing three voltage levels $-V_{in}/2$, 0 and $V_{in}/2$.

Figure 8 shows the steady-state response of the sliding surface s(x), the threshold ±h, and the output current of the inverter i_1 corresponding to $I_2^* = 10A$ (the amplitude of i_2^*). Moreover, it can be seen that the positive cycle of the sliding surface varies from 0 to +h while the negative cycle varies from 0 to $-$h.

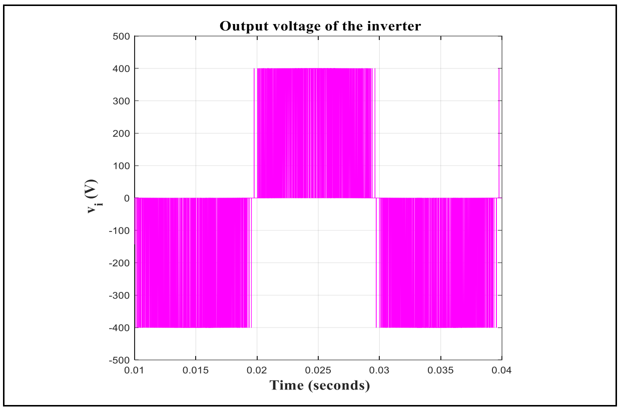

Figure 7: The output voltage of three levels inverter

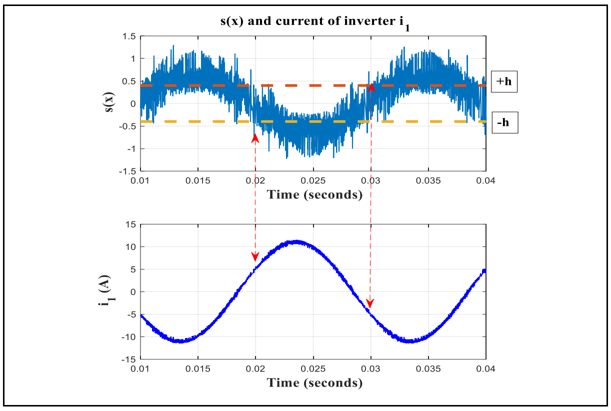

Figure 8: Sliding surface s(x) in steady state and inverter current i1 when $I_2^* = 10A$

It can be observed that the zero point of the sliding surface causes distortion in the inverter current i_1. However, these distortions and harmonic switching in the inverter current i_1 will be filtered out by the LCL filter before interacting with the gird current i_2.

In Figure 9, when $I_2^* = 10A$, the grid current i_2 follows the reference value, and the voltage v_c also closely follows the grid voltage v_g. It can be seen that the voltage v_c and the current i_2 have a sinusoidal shape with very low THD and the compatibility of the measured values with their reference values is very high, indicating the algorithm's effectiveness.The grid current is in phase with the grid voltage, and the compatibility and total harmonic distortion for the voltage v_c and the grid current i_2 are respectively NRMSE = [95.20%, 99.63%], THD = [0.06%, 0.04%].

In Figure 10, when I_2^* changes to 5A, the current i_2 has a sinusoidal shape and follows the reference. Since the grid voltage v_g remains constant, the voltage v_c also remains constant and follows the grid voltage. The compatibility and THD of v_c and i_2 are respectively NRMSE = [97.62%, 99.33%, THD = [0.065%, 0.10%].

When $I_2^* = 10A$ along with the reference of noise distribution $D(t)$ with an amplitude ±100V in the voltage V_{dc}, Figure 11a represents the noise distribution and the phase voltage at the inverter output with three voltage levels: -$V_{in}/2$, 0 and $V_{in}/2$. Figure 11b shows the steady-state response of the sliding surface s(x), threshold level ±h and the inverter current i_1.

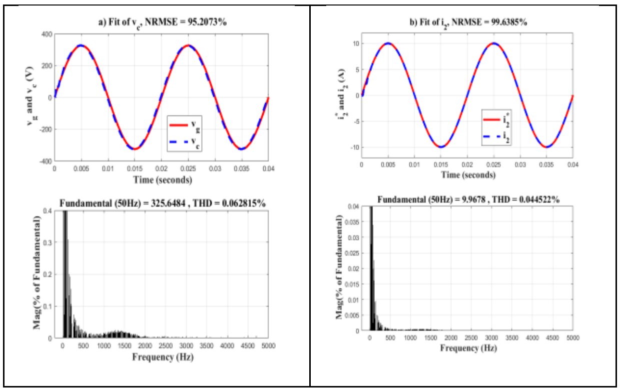

Figure 9: Inverter output response when $I_2^* = 10A$

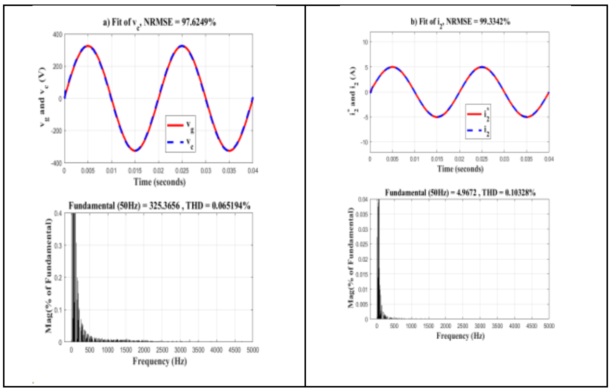

Figure 10: Inverter output response when $I_2^* = 5A$

Similarly, the zero point of the sliding surface also causes distortion in the inverter current. In Figure12, when $I_2^* = 10A$ and $D(t)$ has an amplitude of ±100V, the voltage v_c and the grid current i_2 have a sinusoidal shape and still follow their reference values well.

The current and grid voltage are in phase, with the compatibility and THD of v_c and i_2 are NRMSE = [95.20%, 99.65%], THD = [0.069%, 0.05%], respectively. These values are not affected by the noise due to the effect of the LCL filter, which limits the noise before it is injected into the grid.

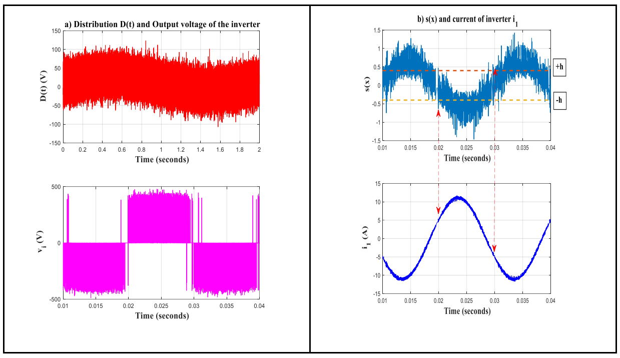

Figure 11: a) Noise distribution $D(t)$ and phase voltage; b) Sliding surface $s(x)$ and inverter current i_1

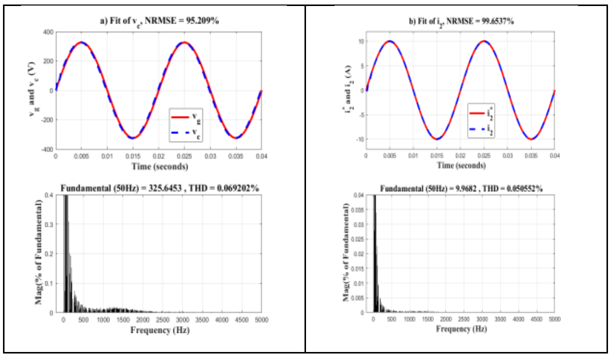

Figure 12: Inverter ouput response with noise $D(t)$

When the reference current I_2^* changes from 5A to 10A at the 1-second mark, Figure 13a shows the steady-state response of the sliding surface $s(x)$, the threshold $\pm h$ and the inverter current i_1. At the zero point of the sliding surface, i_1 is still distorted. In Figure 13b, the grid current i_2 and the voltage v_c have a sinusoidal shape and still follow their reference values.

Figure 14 illustrates the simulation response of $dV(x)/dt$ corresponding to I_2^* changing from 5A to 10A. It can be seen that the derivative of the Lyapunov function is always negative despite the changing reference current, demonstrating that the closed-loop system is globally asymptotically stable. From equation (20) and the simulation result, it can be seen that when α has a small value, the complex conjugate poles are close to the imaginary axis, leading to undesirable oscillations. Conversely, when α has a large value, the complex conjugate poles are far from the imaginary axis, causing i_2 to quickly follow its reference value.

As previously explained, the main objective of adding the term $c_2 \times 2$ into the sliding surface in (10) is to eliminate the steady-state error in the capacitor voltage. The influence of different c_2 values on the steady-state error of the voltage varies.

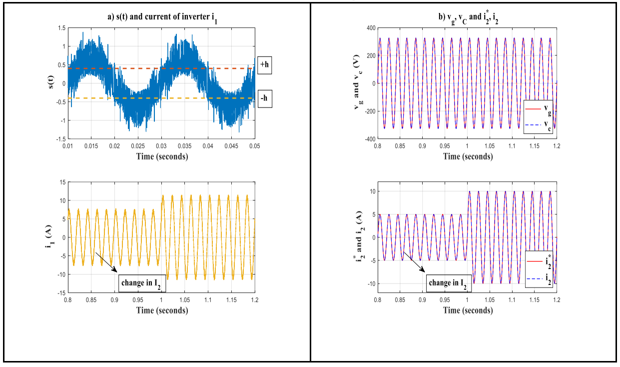

Figure 13: Inverter output response when I_2^* changes from 5A to 10A

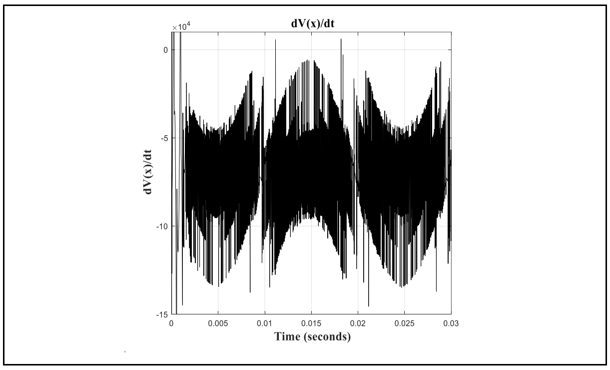

Figure 14: Simulated response of $dV(x)/dt < 0$

3.2 Experimental results

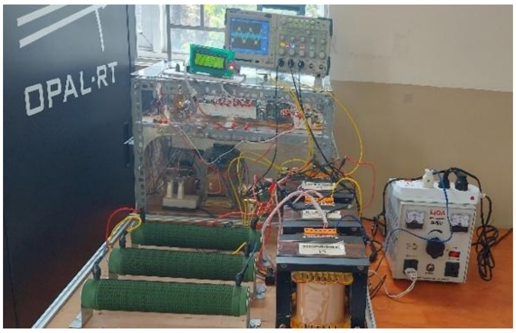

Figure 15: Experimental setup.

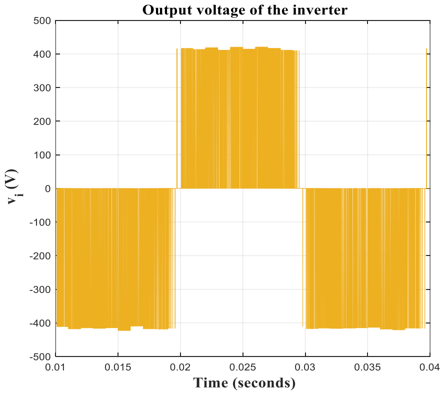

Figure 16: Experimental output of the three-level inverter

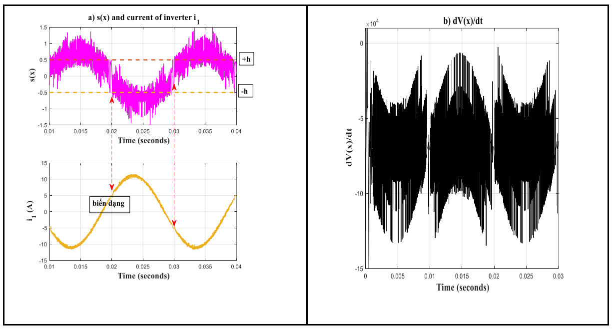

Figure 17: a) Sliding surface s(x), threshold h and the inverter current i1; b) $dV(x)/dt\ <\ 0$

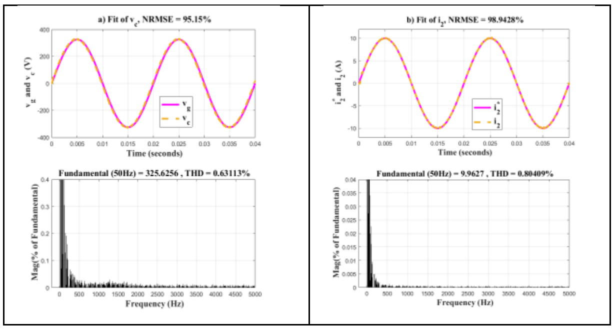

Figure 18: Experimental output of the inverter when $I_2^* = 10A$

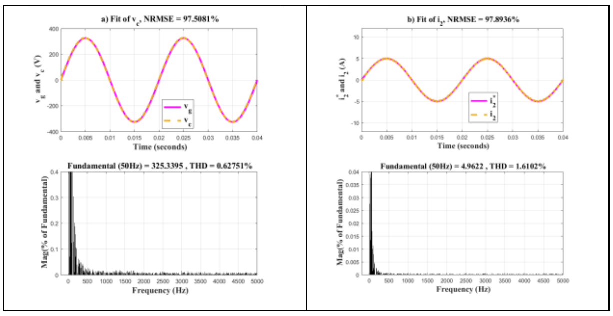

Figure 19: Experimental output of the inverter when $I_2^* = 10A$

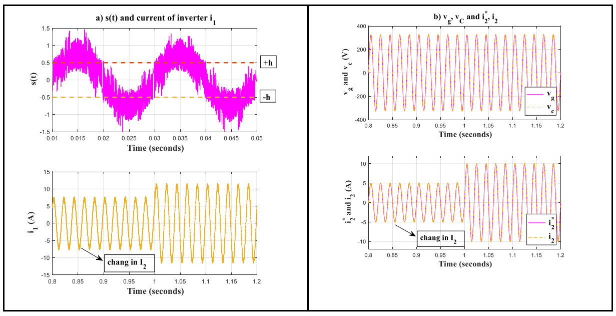

Figure 20. Experiment when I_2^* changes from 5A to 10A

Figure 15 is the real-time experimental setup for a three-level NPC T-Type single phase inverter. The control program is implemented on Matlab/Simulink, and the experimental response of the converter is collected on a computer through the DSP 320F28379. The reference current I_2^* is adjusted using a 1kΩ potentiometer.

Figure 16 illustrates the experimental output voltage of the inverter when using the dual-band hysteresis modulation scheme with three voltage level: -400, 0V and +400V. The overlapping voltage levels are due to the deviation of the hysteresis h in the experiment.

Experiment when $I_2^* = 10A$, Figure17a shows the steady-state response of the sliding $s(x)$, the threshold level ±h, and the inverter current i_1. At the zero point of the sliding surface, it also causes distortion in the inverter current i_1. As simulated, these distortions will be eliminated by the LCL filter before interacting with the grid current i_2. Figure 17b illustrates the experiment of $dV(x)/dt\ < 0$. The derivative of the Lyapunov function is always negative, proving that the closed-loop system is globally asymptotically stable.

Experiment when $I_2^* = 10A$ is indicated in Figure 18. The grid current i_2 and voltage v_c have a sinusoidal shape and are in phase with the grid voltage, closely following their reference values. The compatibility and total harmonic distortion for the voltage v_c and grid current i_2 are NRMSE = [95.15%, 98.94%], THD = [0.63%, 0.8%], respectively.

In Fiugure19, experiment when changing $I_2^* = 5A$. The current i_2 has a sinusoidal shape and follows the set value. Since the grid voltage vg remains constant, the voltage v_c also remains constant and follows the grid voltage. The compatibility and THD of v_C and i_2 are NRMSE = [97.5%, 97.89%], THD = [0.62%, 1.6%], respectively. The differences in THD and NRMSE values compared to the simulation are due to hardware errors.

In the experiment, when the reference current I_2^* changes from 5A to 10A at the 1-second mark, Figure 20a shows the steady-state response of the sliding surface s(x), the threshold ±h and the inverter current i_1. Notably, at the zero point of the sliding surface, the inverter current i_1 was still being distorted. Figure 20b illustrates that the grid current i_2 and the voltage v_c maintained a sinusoidal waveform, adhering closely to the reference values.

4 CONCLUSIONS

This paper successfully designed, developed, and validated a single-phase grid-connected T-type Neutral Point Clamped (T-NPC) inverter using a novel Sliding Mode Control (SMC) strategy with an LCL filter and a dual-band hysteresis switching technique.

The proposed control structure was rigorously modeled and simulated in MATLAB/SIMULINK, and its performance was confirmed through experimental validation. The results clearly demonstrate the effectiveness of the dual-loop control method, achieving precise voltage and current tracking despite variations in the reference current and the presence of external disturbances. This confirms the controller's robust suitability for highly nonlinear systems.

A key contribution of this method is its complete insensitivity to uncertainties and external disturbances, a feature verified by the low harmonic distortion and the high NRMSE compatibility between the measured and reference signals. Furthermore, the stability analysis confirms the asymptotic stability of the system around the equilibrium point. By formulating the sliding surface $s(x)$ based on Equation (10), the system's stability is made dependent only on the constants c_1, c_2 and c_3. This novel formulation allows for the selective placement of the desired pole pair, effectively reducing voltage and current harmonics before injection into the grid, thereby significantly enhancing the controller's robustness and overall system performance.

In summary, the proposed SMC-based control technique offers a simple, highly robust, and effective solution for grid-connected inverters, outperforming conventional methods in terms energy quality and resilience.

ACKNOWLEDGMENT

This work was supported by the Industrial University of Ho Chi Minh City, Vietnam (IUH). The authors would like to thank IUH, the editor, the associate editors and the reviewers for their valuable comments.

REFERENCES

[1]. Nasim Ahmed, Md. Ziaur Rahman Khan, “A Single-Phase Grid-Connected Inverter using Phase Control Method,” *2021 IEEE International Conference in Power Engineering Application (ICPEA)*, 04 October 2021.

[2]. P. A. Pattanaik, N. K. Pilli and S. K. Singh, "Design, simulation & performance evaluation of three phase grid connected PV panel," *2015 IEEE Power, Communication and Information Technology Conference (PCITC), Bhubaneswar*, 2015, pp. 195-200.

[3]. M. Monfared, M. Sanatkar e S. Golestan “Direct active and reactive power control of single-phase grid-tie converters,” *IET Power Electronics*, vol. 5, pp. 1544-1550, 2012.

[4]. H. Cha and T. Vu, "Comparative analysis of low-pass output filter for single-phase grid-connected Photovoltaic inverter," *2010 Twenty- Fifth Annual IEEE Applied Power Electronics Conference and Exposition (APEC), Palm Springs,* CA, 2010, pp. 1659-1665.

[5]. ZHANG Ruiping, LU Hongxia Yang Jie, ZHANG Tingrong," Single-phase Photovoltaic Grid-connected Inverter Current Control Method Based on MRAC," *7th International Conference on Energy, Environment and Sustainable Development (ICEESD),* 2018.

[6]. Channareth Srun, Phok Chrin, Sokchea Am, Bunthern Kim, "Modeling and Simulation of a Double-Stage Single-Phase Grid- Connected PV System," *EPI International Journal of Engineering*, Volume 5, Number 1, February 2022, pp. 16-20.

[7]. R. Ichikawa, H. Funato and K. Nemoto, "Experimental single phase utility interface inverter based on digital hysteresis current controller," *2011 International Conference on Electrical Machines and Systems, Beijing*, 2011, pp.

[8]. P. A. Dahono, "New hysteresis current controller for single-phase full-bridge inverters," *in IET Power Electronics*, vol. 2, no. 5, pp. 585-594, Sept. 2009.

[9]. B. Bahrani, A. Rufer, S. Kenzelmann and L. A. C. Lopes, "Vector Control of Single-Phase Voltage-Source Converters Based on Fictive- Axis Emulation," *in IEEE Transactions on Industry Applications*, vol. 47, no. 2, pp. 831-840, March-April 2011.

[10]. S. Samerchur, S. Premrudeepreechacharn, Y. Kumsuwun and K. Higuchi, "Power control of single-phase voltage source inverter for grid-connected photovoltaic systems," *2011 IEEE/PES Power Systems Conference and Exposition, Phoenix,* AZ, 2011, pp. 1-6.

[11]. M. Ciobotaru, R. Teodorescu, F. Blaabjerg. 'Control of single-stage single-phase PV inverter'. *Proc. IEEE 11th Eur. Conf. on Power Electronics Application, Dresden, Germany*, September 2005, p. 10.

[12]. R. Guzman, L. G. de Vicuña, M. Castilla, J. Miret, and J. de la Hoz, "Variable structure control for three-phase LCL-filtered inverters using a reduced converter model," *IEEE Trans. Ind. Electron*., vol. 65, no. 1, pp. 5–15, Jan. 2018.

[13]. M. Pichan and H. Rastegar, "Sliding-Mode control of four-leg inverter with fixed switching frequency for uninterruptible power supply applications," *IEEE Trans. Ind. Electron*., vol. 64, no. 8, pp. 6805–6814, Aug. 2017.

[14]. Ganguly, Anupama; Biswas, Pabitra Kumar; Gupta, Suraj; Ahmad, Furkan. "Metaheuristic Optimization-Based Sliding Mode Control With Modified Perturb and Observe for Controlling MPPT of a PV Interfaced Grid Connected System" *International Journal of Energy Research*; Bognor Regis Vol. 2025, (2025).

[15] Chang, En-Chih; Rong-Ching, Wu; Chang, Heidi H; Chun-An, Cheng. "A State-Feedback Control Strategy Based on Grey Fast Finite-Time Sliding Mode Control for an H-Bridge Inverter with LC Filter Output," *Electronics*; Basel Vol. 13, Iss. 11, (2024): 2118.

[16]. Muhammet CengizTurgay Duman. "Sliding mode control for a single-phase grid-connected H-bridge NPC inverter with a symmetrical LCL filter," *Computers and Electrical Engineering*, July 2024.

[17]. Rabbani Amir; Dehghani Mahla; Mardaneh Mohammad; Jamshidpour Ehsan; Hasanvand Saeed. "Non-singular Fast Terminal Sliding Mode Control_ Integrated with Proportional Multi-Resonant-Based Controller for Multifunctional Grid-Tied LCL-Filtered Inverter," *Power Electronics and Drives*; Wrocław Vol. 10, Iss. 1, (2025): 257-270.

[18]. H. Komurcugil, S. Ozdemir, I. Sefa, N. Altin, and O. Kukrer, "Sliding-mode control for single-phase grid-connected LCL-filtered VSI with double-band hysteresis scheme," *IEEE Trans. Ind. Electron*., vol. 63, no. 2, pp. 864–873, Feb. 2016.

[19]. Komurcugil, S. Biricik, S. Bayhan, and Z. Zhang, "Sliding mode control: overview of its applications in power converters," *IEEE Ind. Electron. Mag.*, vol. 15, no. 1, pp. 40–49, Mar. 2021.

[20]. Hasan Komurcugil; Sertac Bayhan; Ramon Guzman; Mariusz Malinowski. Design of Lyapunov Function-Based Control of Various Power Converters, Page: 261 – 308, Edition: 1, *Wiley-IEEE Press*, 2023.

PHƯƠNG PHÁP KIỂM SOÁT DÒNG ĐIỆN BIẾN TẦN KẾT NỐI LƯỚI MỘT PHA DỰA TRÊN SMC VỚI BỘ LỌC LCL

PHẠM TRẦN BÍCH THUẬN[1*], NGUYỄN VINH QUAN[2]
[1] Phòng Quản lý khoa học và Hợp tác quốc tế, Trường Đại học Công nghiệp Thành phố Hồ Chí Minh
[2] Khoa Công nghệ Điện tử, Trường Đại học Công nghiệp Thành phố Hồ Chí Minh
Tác giả liên hệ: phamtranbichthuan@iuh.edu.vn

Tóm tắt. Một kỹ thuật điều khiển dòng điện mới cho bộ biến tần đa mức Neutral Point Clamped (NPC) một pha đã được đề xuất, được sử dụng để hòa lưới điện và điều chỉnh điện áp liên kết DC. Thách thức chính là việc điều khiển hệ thống có bộ lọc LCL gây ra hiện tượng cộng hưởng, cùng với khó khăn trong việc tạo ra điện áp tham chiếu cho tụ lọc. Để giải quyết các vấn đề này, một thuật toán Điều khiển Trượt (SMC) mới được giới thiệu, có khả năng triệt tiêu cộng hưởng LCL mà không cần sử dụng phương pháp giảm xóc bổ sung. Hệ thống áp dụng cấu trúc Điều khiển Vòng Lặp Đa Dạng (MLC), bao gồm một vòng điều khiển dòng điện ngoài và một vòng điều khiển điện áp bên trong sử dụng bộ điều khiển tỉ lệ cộng hưởng (PR). Vòng lặp bên trong này giúp giảm thiểu hiệu quả sai số xác lập của điện áp tụ và giảm thiểu hiện tượng rung giật (chattering) do SMC gây ra, từ đó tăng cường hiệu suất và độ bền vững của hệ thống. Ngoài ra, kỹ thuật chuyển mạch băng thông trễ với băng tần kép được sử dụng để tạo xung điều khiển. Kết quả mô phỏng và thực nghiệm trên bộ biến tần NPC loại T ba mức đã xác nhận tính hiệu quả và độ tin cậy của chiến lược điều khiển đề xuất trong các điều kiện thay đổi và có nhiễu loạn.

Từ khóa. Biến tần một pha; Biến tần kẹp điểm trung tính; Điều khiển chế độ trượt; Bộ điều khiển dòng điện.

Received on October 22– 2025

Revised on December 19 – 2025